Fast calculation of the g-functions of geothermal borehole fields using similarities in the evaluation of the finite line source solution

Massimo Cimmino

Département de génie mécanique, Polytechnique Montréal, Montreal, Canada

Département de génie mécanique
Polytechnique Montréal
Case Postale 6079, succursale "centre-ville"
Montreal, Quebec, Canada, H3C 3A7
massimo.cimmino@polymtl.ca

Fast calculation of the g-functions of geothermal borehole fields using similarities in the evaluation of the finite line source solution

Numerical methods are proposed for the efficient evaluation of the g-functions of geothermal bore fields using the finite line source solution. The presented methods reduce the calculation time for the calculation of g-functions by reducing the number of numerical evaluations of the analytical finite line source solution. A similarity identification method is presented to identify pairs of boreholes for which the finite line source solution takes the same value. A load history reconstruction method is presented to evaluate the g-function at non-uniform time-steps. Using the proposed numerical methods, the calculation time for the g-function of a rectangular field of 12 × 12 boreholes is reduced by a factor 308. The numerical methods allow the evaluation of g-functions of bore fields with large amounts of boreholes in irregular configurations. The g-function of a field of 512 randomly positioned boreholes is calculated in 27 minutes.

Keywords: Geothermal boreholes; Ground heat exchangers; g-Functions; Thermal response factors; Finite line source.

Nomenclature

Variables

α_s	Soil thermal diffusivity
B	Borehole spacing
ΔT_b	Borehole wall temperature drop
D	Borehole buried depth
d	Separating distance
g	g-Function
h^{real}, h^{image}	Real and image thermal response factor
h, h_q	Total thermal response factor
k_s	Soil thermal conductivity
L, L_q	Borehole or borehole segment length
L_{tot}	Total borehole length
N_b	Total number of boreholes
N_d	Total number of distance groups
N_q	Total number of borehole segments
$N_{s,real}$, $N_{s,image}$	Number of real and image similarity groups
N_t	Number of time-steps
n_q	Number of segments per borehole
$n_{s,real}$, $n_{s,image}$	Number of segment pairs in a similarity group
Φ'_q	Reconstructed load history
$\bar{Q}'_b$	Average heat extraction rate per unit borehole length
Q'_b	Heat extraction rate per unit borehole length
$\tilde{Q}'_b$, $\tilde{Q}'_q$	Normalized heat extraction rate per unit borehole length
r_b, r_q	Borehole radius
Θ_b, Θ_q	Dimensionless borehole wall temperature
$\bar{T}_b$	Average borehole wall temperature
T_b	Borehole wall temperature
T_g	Undisturbed ground temperature

τ	Dimensionless time
t	Time
t_s	Bore field characteristic time
(x, y)	Borehole coordinates

Matrices and vectors

$\boldsymbol{H_b}$, $\boldsymbol{H_q}$	Matrix of segment-to-segment thermal response factors
$\boldsymbol{L}^*$	Vector of segment length fractions
$\boldsymbol{\Phi}'_{\boldsymbol{q}}$	Vector of reconstructed load histories of borehole segments
$\boldsymbol{Q}'_{\boldsymbol{b}}$, $\boldsymbol{Q}'_{\boldsymbol{q}}$	Vector of heat extraction rates per unit borehole length
$\widetilde{\boldsymbol{Q}}'_{\boldsymbol{b}}$, $\widetilde{\boldsymbol{Q}}'_{\boldsymbol{q}}$	Vector of normalized heat extraction rates per unit borehole length
$\boldsymbol{\Theta_b}$, $\boldsymbol{\Theta_q}$	Vector of dimensionless borehole segment temperatures
$\boldsymbol{T_b}$, $\boldsymbol{T_q}$	Vector of borehole segment temperatures

Indices

i, j	Borehole indices
k	Time-step index
m, n	Cumulative borehole segment indices
u, v	Borehole segment indices

Superscripts

0	Values assuming no heat extraction during current time-step

1. Introduction

The simulation of ground source heat pump systems aims at predicting the returning fluid temperatures from geothermal boreholes and the ground temperatures in the bore field. The accurate prediction of these temperatures is critical to the evaluation of the ground source heat pump performance and to the proper design of the system. Temperatures in the bore field can be

obtained by the temporal superposition of thermal response factors, which give the relation between the ground temperature at the borehole walls and the overall heat extraction rate in the bore field.

Eskilson (1987) introduced three-dimensional thermal response factors, also known as g-functions, to evaluate borehole wall temperatures in geothermal bore fields. Since heat extraction within the boreholes is driven by the difference between the heat carrier fluid temperature and the borehole wall temperature and, additionally, that the fluid temperature change within the borehole is relatively small (e.g. 3°C to 5°C), it was recognized that the heat extraction from a borehole could be approximated by a cylinder at uniform temperature. g-Functions were obtained numerically using a finite difference method. Each borehole was modelled in a two-dimensional radial-axial grid. At each time-step of the simulation, the total temperature variation at the borehole walls was evaluated by spatial superposition of the temperature grids around every borehole. The heat extraction rates at each node along the boreholes required to obtain a uniform borehole wall temperature were evaluated. The g-function of a bore field is defined by the following relation:

$$\bar{T}_b(t/t_s) = T_g - \frac{\bar{Q}'_b}{2\pi k_s} g(t/t_s) \qquad (1)$$

where $\bar{T}_b$ is the average borehole wall temperature in the bore field, T_g is the undisturbed ground temperature, k_s is the ground thermal conductivity, $\bar{Q}'_b$ is the average heat extraction rate per unit borehole length in the bore field and g is the g-function.

The g-function is dependent on the dimensionless parameters of the bore field, namely: the dimensionless borehole radius r_b/L, the dimensionless borehole spacing B/L, the dimensionless buried depth D/L and the dimensionless time t/t_s, where $t_s = L^2/(9\alpha_s)$ is the

bore field characteristic time and α_s is the ground thermal diffusivity. g-Functions are usually presented for a given value of the dimensionless borehole radius and the dimensionless buried depth, as shown on Figure 1 for a rectangular field of 5 × 5 boreholes. Once the g-function for a bore field is known, the borehole wall temperature variation to a variable heat extraction rate is obtained by temporal superposition of the g-function.

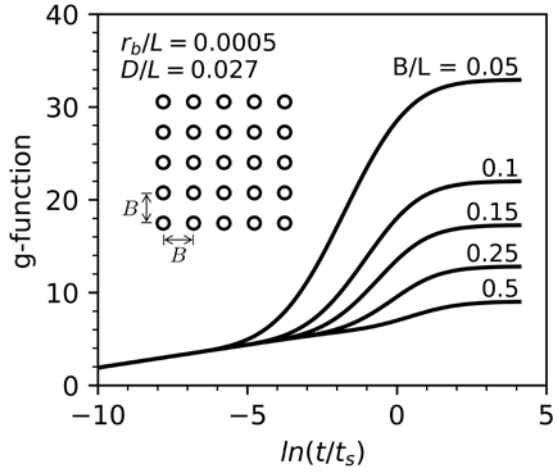

Figure 1. g-Functions of a rectangular field of 5 × 5 boreholes

g-Functions are implemented into several software tools for the sizing and the simulation of ground-source heat pump systems (Hellström and Sanner 1994; Spitler 2000; Fisher et al. 2006; Liu and Hellström 1999), where they are often tabulated. When the values of the dimensionless parameters of a bore field of interest are in between the tabulated values implemented into the software, the g-function is interpolated. This process may lead to errors in the g-function values (Malayappan and Spitler 2013). Tabulated g-functions are also limited to predetermined configurations of boreholes in a bore field. It is then beneficial to generate the g-function for the bore field of interest rather than use tabulated values.

Numerical methods like that of Eskilson to evaluate g-functions are difficult to implement and their solution is time consuming for fields with large amounts of boreholes.

Eskilson proposed the use of the finite line source analytical solution to estimate the value of the g-function for a single vertical borehole. Zeng et al. (2002) proposed the spatial superposition of the finite line source solution to calculate thermal response factors for bore fields. Their solution, however, required the numerical evaluation of a double integral. Simplified single integral forms of the finite line source solution were proposed by Lamarche and Beauchamp (2007) and Claesson and Javed (2011).

The finite line source solution has been extended beyond vertical boreholes in homogenous isotropic ground connected in parallel. Cui et al. (2006) proposed a finite line source solution for inclined boreholes. Marcotte and Pasquier (2009) later investigated the case of inclined boreholes with non-zero buried depth. Considerations for the efficient evaluation of the inclined finite line source solution were analysed by Lamarche (2011). Molina-Giraldo et al. (2011) introduced the moving finite line source solution to account for groundwater advection around the boreholes. Li and Lai (2012) formulated the finite line source solution for anisotropic ground thermal properties. Abdelaziz et al. (2014) and, later, Hu (2017) considered the case of multi-layered ground with different thermal properties. Marcotte and Pasquier (2014) coupled the finite line source solution to an effective thermal resistance model of the boreholes to evaluate thermal response factors of bore fields with mixed parallel-series connections.

Finite line source methods tend to overestimate Eskilson's g-functions, especially for closely packed bore fields with many boreholes as evidenced, for instance, by Fossa (2011). These differences are mainly due to the differences in the boundary conditions at the borehole wall (Cimmino, Bernier, and Adams 2013). The finite line source solution represents the boreholes as line sources with uniform heat extraction along their length, whereas Eskilson considered cylinder sources with uniform temperature. To correct the differences between the

finite line source solution and Eskilson's g-functions, Cimmino and Bernier (2014) modeled the boreholes as series of finite line source segments. The finite line source segments were superposed spatially and temporally to obtain a uniform temperature along the boreholes, equal for all boreholes. The thermal response factors generated using their method were successfully validated against Eskilson's g-functions for rectangular bore fields ranging from a single borehole to an array of 12 × 12 boreholes. Using the same method, Lazzarotto and Björk (Lazzarotto 2016; Lazzarotto and Björk 2016) used the finite line source solution to estimate g-functions of fields of inclined boreholes. Lamarche (2017b) considered a piecewise-linear variation of the heat extraction rates along the line source segments to evaluate g-functions. Cimmino (2015) verified the validity of the uniform temperature boundary condition by coupling the finite line source segment method to an analytical solution of the fluid temperature variation inside the boreholes. The model was used to evaluate thermal response factors for equal inlet fluid temperature, considering the axial variation of the borehole wall temperatures and heat extraction rates. It was shown that the thermal response factors approach the thermal response factors obtained considering uniform borehole wall temperatures as the borehole thermal resistance decreases.

An issue with using series of finite line source segments to model the boreholes is that it significantly increases the computational time for the evaluation of the thermal response factors. The computational time is approximately proportional to the square of finite line sources in the bore field. Using 12 finite line source segment per borehole, as recommended by Cimmino and Bernier (2014), the computational time increases by a factor 144. For very large bore fields, the computational time for the evaluation of the thermal response factors can be several hours. This paper addresses this issue by introducing numerical methods to reduce the number of required

evaluations of the finite line source solution: a similarity identification method and a load history reconstruction method are presented.

2. Mathematical model

Figure 2 shows a field of $N_b = 3$ vertical boreholes connected in parallel. Each borehole i has a radius $r_{b,i}$, a length L_i and is buried at a distance D_i from the ground surface. The ground has a thermal conductivity k_s and a ground thermal diffusivity α_s. The g-function of the bore field is obtained by evaluating the overall average (over the length) borehole wall temperature in the bore field for a constant total heat extraction rate from the bore field (Equation (1)).

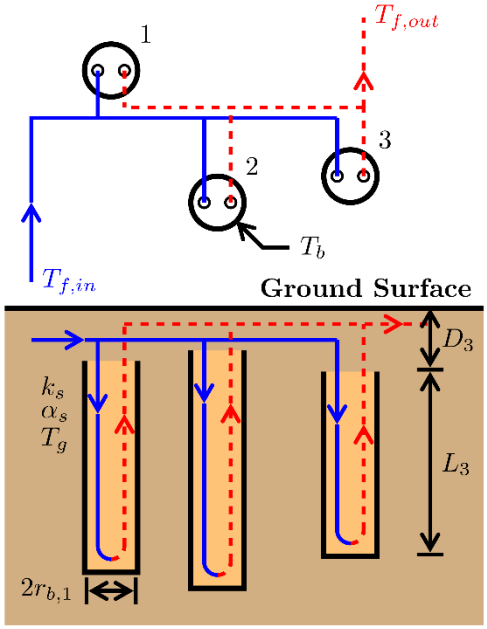

Figure 2. Field of 3 vertical boreholes

Each borehole i is divided into $n_{q,i}$ segments of equal length. The ground temperature drop around any borehole segment is calculated by adding the contributions of a "real" line source segment located along the axis of the borehole segment and an "image" line source segment of opposite sign located above ground and mirrored with regards to the ground surface.

This image line source ensures that there is no temperature variation at the ground surface. The superposition of real and image line sources is illustrated in Figure 3.

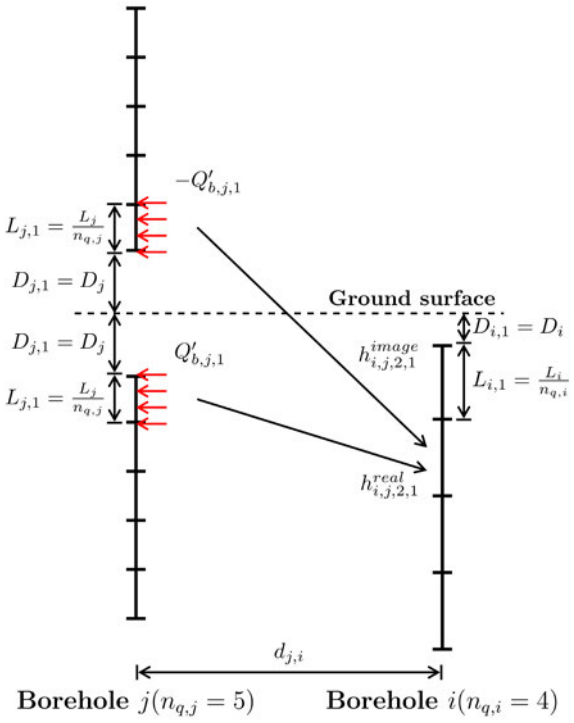

Figure 3. Spatial superposition of real and image line sources

For a segment u of a borehole i, the temperature drop due to constant heat extraction per unit borehole length $Q'_{b,j,v}$ at a segment v of a borehole j, starting at time $t = 0$, is obtained by averaging the temperature drop over the length of segment u of borehole i caused by the real and image line segments corresponding to segment v of borehole j (Cimmino and Bernier 2014):

$$\Delta T_{b,i,j,u,v}(t) = \frac{1}{2\pi k_s}\left(h^{real}_{i,j,u,v}(t) + h^{image}_{i,j,u,v}(t)\right) Q'_{b,j,v} \tag{2}$$

$$h^{real}_{i,j,u,v}(t) = \frac{1}{2L_{i,u}} \int_{1/\sqrt{4\alpha_s t}}^{\infty} \frac{1}{s^2} \exp\left(-d^2_{i,j} s^2\right) I^{real}_{FLS}(s) ds \tag{3}$$

$$I_{FLS}^{real}(s) = \text{erfint}\Big(\big(D_{i,u} - D_{j,v} + L_{i,u}\big)s\Big) - \text{erfint}\Big(\big(D_{i,u} - D_{j,v}\big)\text{s}\Big) + \text{erfint}\Big(\big(D_{i,u} - D_{j,v} - L_{j,v}\big)s\Big) - \text{erfint}\Big(\big(D_{i,u} - D_{j,v} + L_{i,u} - L_{j,v}\big)s\Big) \quad (4)$$

$$h_{i,j,u,v}^{image}(t) = \frac{1}{2L_{i,u}} \int_{1/\sqrt{4\alpha_s t}}^{\infty} \frac{1}{s^2} \exp\big(-d_{i,j}^2 s^2\big)\, I_{FLS}^{image}(s) ds \quad (5)$$

$$I_{FLS}^{image}(s) = \text{erfint}\Big(\big(D_{i,u} + D_{j,v} + L_{i,u}\big)s\Big) - \text{erfint}\Big(\big(D_{i,u} + D_{j,v}\big)s\Big) + \text{erfint}\Big(\big(D_{i,u} + D_{j,v} + L_{j,v}\big)s\Big) - \text{erfint}\Big(\big(D_{i,u} + D_{j,v} + L_{i,u} + L_{j,v}\big)s\Big) \quad (6)$$

$$\text{erfint}(X) = \int_0^X \text{erf}(x')\, dx' = X\,\text{erf}(X) - \frac{1}{\sqrt{\pi}}\big(1 - \exp(-X^2)\big) \quad (7)$$

$$d_{i,j} = \begin{cases} r_{b,i} & \text{for } i = j \\ \sqrt{\big(x_i - x_j\big)^2 + \big(y_i - y_j\big)^2} & \text{for } i \neq j \end{cases} \quad (8)$$

where $\Delta T_{b,i,j,u,v}$ is the borehole wall temperature drop at segment u of borehole i due to constant heat extraction at segment v of borehole j, $h_{i,j,u,v}^{real}$ and $h_{i,j,u,v}^{image}$ are the real and image segment-to-segment thermal response factors of segment v of borehole j over segment u of borehole i, $d_{i,j}$ is the radial distance between borehole i and borehole j.

The borehole wall temperature at segment u of borehole i is obtained by adding the contributions of all borehole segments. For a constant heat extraction at all segments of all boreholes:

$$T_{b,i,u}(t) = T_g - \sum_{j=1}^{N_b} \sum_{v=1}^{n_{q,j}} \frac{1}{2\pi k_s} h_{i,j,u,v}(t)\, Q'_{b,j,v} \quad (9)$$

where $T_{b,i,u}$ is the borehole wall temperature at segment u of borehole i, T_g is the initial ground temperature and $h_{i,j,u,v}(t) = h_{i,j,u,v}^{real}(t) + h_{i,j,u,v}^{image}(t)$ is the total segment-to-segment thermal

response factor of segment v of borehole j over segment u of borehole i.

For time-varying heat extraction rates at all segments of all boreholes, the borehole wall temperature is obtained by temporal superposition:

$$T_{b,i,u}(t_k) = T_g - \sum_{j=1}^{N_b} \sum_{v=1}^{n_{q,j}} \sum_{k'=1}^{k} \frac{1}{2\pi k_s} \left(h_{i,j,u,v}(t_k - t_{k'-1}) - h_{i,j,u,v}(t_k - t_{k'}) \right) Q'_{b,j,v}(t_{k'}) \tag{10}$$

where $Q'_{b,j,v}$ is the step-wise constant heat extraction rate per borehole length of segment v of borehole j, with $Q'_{b,j,v}(t_{k'})$ the constant heat extraction rate over the period $t_{k'-1} < t \leq t_{k'}$, $t_0 = 0$ is the initial time and $Q'_{b,j,v}(t_0) = 0$.

Equation (10) can be conveniently expressed in matrix notation:

$$\boldsymbol{T_b}(t_k) = T_g - \sum_{k'=1}^{k} \frac{1}{2\pi k_s} \left(\boldsymbol{H_b}(t_k - t_{k'-1}) - \boldsymbol{H_b}(t_k - t_{k'}) \right) \boldsymbol{Q'_b}(t_{k'}) \tag{11}$$

$$\boldsymbol{T_b}(t_k) = \begin{bmatrix} \boldsymbol{T_{b,1}}(t_k) \\ \vdots \\ \boldsymbol{T_{b,N_b}}(t_k) \end{bmatrix}, \ \boldsymbol{T_{b,i}}(t_k) = \begin{bmatrix} T_{b,i,1}(t_k) \\ \vdots \\ T_{b,i,n_{q,i}}(t_k) \end{bmatrix} \tag{12}$$

$$\boldsymbol{Q'_b}(t_k) = \begin{bmatrix} \boldsymbol{Q'_{b,1}}(t_k) \\ \vdots \\ \boldsymbol{Q'_{b,N_b}}(t_k) \end{bmatrix}, \ \boldsymbol{Q'_{b,i}}(t_k) = \begin{bmatrix} Q'_{b,i,1}(t_k) \\ \vdots \\ Q'_{b,i,n_{q,i}}(t_k) \end{bmatrix} \tag{13}$$

$$\boldsymbol{H_b}(t_k) = \begin{bmatrix} \boldsymbol{H_{b,1,1}}(t_k) & \cdots & \boldsymbol{H_{b,1,N_b}}(t_k) \\ \vdots & \ddots & \vdots \\ \boldsymbol{H_{b,N_b,1}}(t_k) & \cdots & \boldsymbol{H_{b,N_b,N_b}}(t_k) \end{bmatrix}, \ \boldsymbol{H_{b,i,j}}(t_k) = \begin{bmatrix} h_{i,j,1,1}(t_k) & \cdots & h_{i,j,1,n_{q,i}}(t_k) \\ \vdots & \ddots & \vdots \\ h_{i,j,n_{q,i},1}(t_k) & \cdots & h_{i,j,n_{q,i},n_{q,i}}(t_k) \end{bmatrix} \tag{14}$$

where $\boldsymbol{T_b}$ is a column vector of the borehole wall temperatures at all segments of all boreholes, $\boldsymbol{Q'_b}$ is a column vector of the heat extraction rates per borehole length at all segments of all

boreholes and $\boldsymbol{H_b}$ is the matrix of the segment-to-segment thermal response factors.

The borehole wall temperatures are calculated time-step by time-step, starting from t_1. At any time t_k, previous values of $\boldsymbol{T_b}$ and $\boldsymbol{Q'_b}$ are known. It is then appropriate to cast Equation (11) based only on values of these variables for the current time-step:

$$\boldsymbol{T_b}(t_k) = \boldsymbol{T_b^0}(t_k) - \frac{1}{2\pi k_s}\boldsymbol{H_b}(t_k - t_{k-1})\boldsymbol{Q'_b}(t_k) \tag{15}$$

$$\boldsymbol{T_b^0}(t_k) = T_g - \sum_{k'=1}^{k-1}\frac{1}{2\pi k_s}\big(\boldsymbol{H_b}(t_k - t_{k'-1}) - \boldsymbol{H_b}(t_k - t_{k'})\big)\boldsymbol{Q'_b}(t_{k'}) \tag{16}$$

where $\boldsymbol{T_b^0}(t_k)$ is a column vector of the borehole wall temperatures at all segments of all boreholes at time t_k, assuming zero heat extraction at all segments over the time period $t_{k-1} < t \leq t_k$.

Equations (15) and (16) are rewritten in dimensionless form. Nondimensionalization of temperatures $\boldsymbol{T_b}$ and heat extraction rates $\boldsymbol{Q'_b}$ is done with regards to the constant average heat extraction rate per borehole length in the bore field $\bar{Q}'_b$. Dimensionless temperatures are then given by $\boldsymbol{\Theta_b} = \big(T_g - \boldsymbol{T_b}\big)/(\bar{Q}'_b/2\pi k_s)$ and normalized heat extraction rates by $\widetilde{\boldsymbol{Q}}'_{\boldsymbol{b}} = \boldsymbol{Q'_b}/\bar{Q}'_b$. The dimensionless time is given by $\tau = t/t_s$, where $t_s = 9L^2/\alpha_s$ is the characteristic time of the bore field. The dimensionless form of Equations (15) and (16) are given by:

$$\boldsymbol{\Theta_b}(\tau_k) = \boldsymbol{\Theta_b^0}(\tau_k) + \boldsymbol{H_b}(\tau_k - \tau_{k-1})\widetilde{\boldsymbol{Q}}'_{\boldsymbol{b}}(\tau_k) \tag{17}$$

$$\boldsymbol{\Theta_b^0}(\tau_k) = \sum_{k'=1}^{k-1}\big(\boldsymbol{H_b}(\tau_k - \tau_{k'-1}) - \boldsymbol{H_b}(\tau_k - \tau_{k'})\big)\widetilde{\boldsymbol{Q}}'_{\boldsymbol{b}}(\tau_{k'}) \tag{18}$$

From the definition of the g-function (Equation (1)), the g-function of the bore field is calculated from the average temperature along all segments in the bore field with constant total heat extraction:

$$g(\tau_k) = \frac{\sum_{i=1}^{N_b} \sum_{u=1}^{n_{q,i}} L_{i,u} \Theta_{b,i,u}(\tau_k)}{L_{tot}} \tag{19}$$

where $L_{tot} = \sum_{i=1}^{N_b} L_i$ is the total length of the boreholes in the bore field.

Different considerations for temperature and heat extraction rate profiles along the boreholes lead to different values of the g-function. Three boundary conditions are found in the literature: (1) uniform and equal heat extraction rates along the boreholes (Zeng, Diao, and Fang 2002), (2) uniform and equal temperatures along the boreholes (Cimmino and Bernier 2014) and (3) equal inlet fluid temperatures into the boreholes (Cimmino 2015). Only boundary condition (2) is considered here to demonstrate the numerical methods presented in the next section. Boundary condition (1) is not suitable for demonstration as it does not require any temporal superposition of heat extraction rates (Equations (17) and (18)). The numerical methods presented in this paper are readily applicable to boundary condition (3) and yield similar ameliorations in terms of computational efficiency.

In accordance with boundary condition (2), all borehole segments have equal values of borehole wall temperature $\Theta_b(\tau_k) = \boldsymbol{\Theta_b}(\tau_k)$. For a constant total heat extraction rate in the bore field, the uniform borehole wall temperature in the bore field is obtained by the solution of the following system of equations:

$$\begin{bmatrix} \boldsymbol{H_b}(\tau_k - \tau_{k-1}) & -\mathbf{1}_{N_q \times 1} \\ \boldsymbol{L}^* & 0 \end{bmatrix} \begin{bmatrix} \widetilde{\boldsymbol{Q}}'_{\boldsymbol{b}}(\tau_k) \\ \Theta_b(\tau_k) \end{bmatrix} = \begin{bmatrix} -\boldsymbol{\Theta}^{\mathbf{0}}_{\boldsymbol{b}}(\tau_k) \\ 1 \end{bmatrix} \tag{20}$$

where $\boldsymbol{L}^*$ is a line vector of the length fractions of each of the borehole segments in the bore field, given by:

$$\boldsymbol{L}^* = [\boldsymbol{L}^*_{\mathbf{1}} \quad \cdots \quad \boldsymbol{L}^*_{\boldsymbol{N_b}}], \; \boldsymbol{L}^*_{\boldsymbol{i}} = \left[\frac{L_{i,1}}{L_{tot}} \quad \cdots \quad \frac{L_{i,n_{q,i}}}{L_{tot}}\right] \tag{21}$$

The solution to Equation (20) gives the normalized heat extraction rates and the uniform dimensionless borehole wall temperature in the bore field, which by definition is equal to the g-function (Equation (1)).

3. Numerical methods

The calculation of g-functions follows a two-step process: (1) the construction of the segment-to-segment thermal response factor matrix $\boldsymbol{H_b}$, and (2) the solution of the system of equations (Equation (20)). Step 1 is the most computationally demanding, since it requires the numerical integration of the finite line source solution (Equations (3) and (5)) for all pairs of the $N_q = \sum_{i=1}^{N_b} n_{q,i}$ line sources in the bore field. Also, the segment-to-segment thermal response factor matrix needs to be known for all values of times involved in the temporal superposition of heat extraction rates (Equations (17) and (18)). The total computational time for the calculation of g-functions is strongly tied to the number of evaluations of the finite line source solution. Thus, changes are proposed for the two steps to reduce the number of evaluations of the finite line source solution and thereby reduce the total computational time for the calculation of g-functions. First, a method is described to identify pairs of line source segments for which the numerical integration of the finite line source solution yields the same value. Then, a load history reconstruction method, analogous to load aggregation methods (Bernier et al. 2004; Liu 2005; Claesson and Javed 2012), is presented. This method allows for the evaluation of the segment-to-segment thermal response factors only at selected times t_k and for the use of a variable time-step in the calculation of the g-function.

For the numerical methods detailed in this section, it is convenient to formulate the dimensionless temperature, the normalized heat extraction rate vectors and the thermal response

factor matrix in terms of a cumulative segment index in the bore field, rather than indices for segments and boreholes:

$$\boldsymbol{\Theta_q}(\tau_k) = \boldsymbol{\Theta_b}(\tau_k) \tag{22}$$

$$\Theta_{q,m}(\tau_k) = \Theta_{b,i,u}(\tau_k),\ m = u + \sum_{i'=1}^{i-1} n_{q,i'} \tag{23}$$

$$\widetilde{\boldsymbol{Q}}'_{\boldsymbol{q}}(\tau_k) = \widetilde{\boldsymbol{Q}}'_{\boldsymbol{b}}(\tau_k) \tag{24}$$

$$\tilde{Q}'_{q,m}(\tau_k) = \tilde{Q}'_{b,i,u}(\tau_k),\ m = u + \sum_{i'=1}^{i-1} n_{q,i'} \tag{25}$$

$$\boldsymbol{H_q}(\tau_k) = \boldsymbol{H_b}(\tau_k) \tag{26}$$

$$h_{q,m,n}(\tau_k) = h_{i,j,u,v}(\tau_k),\ m = u + \sum_{i'=1}^{i-1} n_{q,i'},\ n = v + \sum_{j'=1}^{j-1} n_{q,j'} \tag{27}$$

where $\Theta_{q,m}$ is the dimensionless temperature of the m-th segment in the bore field, $\tilde{Q}'_{q,m}$ is the normalized heat extraction rate of the m-th segment in the bore field and $h_{q,m,n}$ is the segment-to-segment thermal response factor of the n-th segment on the m-th segment. This m-th segment has a length $L_{q,m} = L_{i,u}$, a radius $r_{q,m} = r_{b,i}$, is buried at a depth $D_{q,m} = D_{i,u}$ from the ground surface and positioned at coordinate $(x_{q,m},\ y_{q,m})$.

3.1. Similarities in the evaluation of the finite line source solution

At any time τ, the segment-to-segment thermal response factor matrix $\boldsymbol{H_q}(\tau)$ comprises N_q^2 values that must be evaluated by the finite line source solution (Equations (3) and (5)), which includes the numerical evaluation of an integral. Since the integral of the error function is even (i.e. $\mathrm{erfint}(-X) = \mathrm{erfint}(X)$), it can be shown that pairs (m, n) and (n, m) are related by the following property:

$$h_{q,n,m}^{real}(\tau) = \frac{L_{q,m}}{L_{q,n}} h_{q,m,n}^{real}(\tau) \tag{28}$$

$$h_{q,n,m}^{image}(\tau) = \frac{L_{q,m}}{L_{q,n}} h_{q,m,n}^{image}(\tau) \tag{29}$$

This property reduces the number of evaluations of the finite line source solution from N_q^2 to $\frac{1}{2}N_q(N_q+1)$.

To further reduce the number of evaluations of the finite line source solution, conditions are identified for which two pairs of segments (m,n) and (m',n') yield the same value of the segment-to-segment response factor. Here, we define that there is a *similarity* in the evaluation of the real (Equation (3)) or image (Equation (5)) segment-to-segment thermal response factor if the two pairs of segments yield the same value, that is if $h_{q,m,n}^{real}(\tau) = h_{q,m',n'}^{real}(\tau)$ or $h_{q,m,n}^{image}(\tau) = h_{q,m',n'}^{image}(\tau)$, respectively.

By inspection of Equations (3) and (5), conditions are identified for similarities in the evaluation of the finite line source solution. There is a similarity in the evaluation of the real segment-to-segment thermal response factor if the following conditions are met:

(R1) The distances between the two pairs (m,n) and (m',n') are equal:

$$d_{q,m,n} = d_{q,m',n'} \tag{30}$$

$$d_{q,m,n} = \begin{cases} r_{q,m} & \text{for } m = n \\ \sqrt{\left(x_{q,m} - x_{q,n}\right)^2 + \left(y_{q,m} - y_{q,n}\right)^2} & \text{for } m \neq n \end{cases} \tag{31}$$

and (R2) their lengths and difference of buried depths are equal:

$$L_{q,m} = L_{q,m'},\ L_{q,n} = L_{q,n'} \tag{32}$$

$$D_{q,m} - D_{q,n} = D_{q,m'} - D_{q,n'} \tag{33}$$

There is a similarity in the evaluation of the image segment-to-segment thermal response factor if the following conditions are met:

(I1) The distances between the two pairs (m, n) and (m', n') are equal:

$$d_{q,m,n} = d_{q,m',n'} \tag{34}$$

and (I2) their lengths and sum of buried depths are equal:

$$L_{q,m} = L_{q,m'},\ L_{q,n} = L_{q,n'} \tag{35}$$

$$D_{q,m} + D_{q,n} = D_{q,m'} + D_{q,n'} \tag{36}$$

From this property and the similarities, it is possible to reduce considerably the number of evaluations of the finite line source solution. For any pair (m, n), the real segment-to-segment thermal response factor $h_{q,m,n}^{real}(\tau)$ can be applied to all pairs (m', n') that satisfy conditions (R1) and (R2) and then used to calculate the values for pairs (n, m) and (n', m'). The same can be done for image segment-to-segment response factors using conditions (I1) and (I2).

Note that condition (R1) and (I1) are equivalent. For this reason, the identification of similarities is separated into two steps and precedes the evaluation of segment-to-segment thermal response factors. First, pairs of segments are divided into groups that have the same distance $d_{q,m,n}$. Then, similarities are identified within each of the distance groups for the real and image thermal response factors according to conditions (R2) and (I2). Finally, the segment-to-segment thermal response factors are calculated using Equations (3) and (5) for each similarity group and applied to all pairs within the similarity group.

The algorithms for the identification of distance groups, for the identification of similarity groups and for the evaluation of segment-to-segment thermal response factors are detailed in Algorithms 1, 2 and 3 in appendix. Algorithm 1 divides the segment pairs into N_d distance groups. Algorithm 2 further divides each distance group w into $N_{s,real}^{(w)}$ and $N_{s,image}^{(w)}$ similarity groups for the real and image segment-to-segment thermal response factors, respectively. Algorithm 3 evaluates the segment-to-segment thermal response factors. Using the method presented in this section, the number of evaluations of the finite line source solution is $\sum_{w=1}^{N_d} N_{s,real}^{(w)}$ and $\sum_{w=1}^{N_d} N_{s,image}^{(w)}$ for the real and image thermal response factors.

3.2. Load history reconstruction

To build and solve the system of equations in Equation (20), it is necessary to evaluate the matrix of the segment-to-segment response factors $\boldsymbol{H_q}(\tau)$ at all times $\tau_k - \tau_{k'}$ and $\tau_k - \tau_{k'-1}$. When using an uneven time-step (i.e. $\tau_k - \tau_{k-1} \neq cst$), it is then needed to evaluate the thermal response factors at intermediate times $\tau \neq \tau_k$. As was done in the previous section, additional computational time savings can be achieved by decreasing the number of evaluations of the finite line source solution (Equations (3) and (5)). Cimmino and Bernier (2013) suggested to evaluate the thermal response factors only at times τ_k and to estimate the values of the thermal response factors at intermediate times using cubic spline interpolation. This method, however, necessitates the interpolation by cubic splines for all N_q^2 values of the thermal response factors at each evaluated time value and thereby limits the computational efficiency of the method for very large bore fields with large numbers of segments.

A load history reconstruction method is introduced here. The method consists in reconstructing the load history every time-step so that the values of thermal response factors are

only required at times τ_k for the temporal superposition process (Equation (18)). The temporal superposition of the reconstructed heat extraction rates is given by:

$$\boldsymbol{\Theta}_{\boldsymbol{q}}^{\boldsymbol{0}}(\tau_k) = \sum_{k'=1}^{k} \left(\boldsymbol{H}_{\boldsymbol{q}}(\tau_{k'}) - \boldsymbol{H}_{\boldsymbol{q}}(\tau_{k'-1}) \right) \boldsymbol{\Phi}'_{\boldsymbol{q},\boldsymbol{k}}(\tau_k - \tau_{k'}) \tag{37}$$

where $\boldsymbol{\Phi}'_{\boldsymbol{q},\boldsymbol{k}}$ is the reconstructed heat extraction rate at time τ_k.

The reconstructed heat extraction rate is obtained by linear interpolation of the accumulated heat extracted from the bore field, as illustrated in Figure 4 at a time τ_5. The accumulated heat extracted is calculated by the time integration of the heat extraction rates up until time τ_{k-1}:

$$f_{q,k,m}(\tau) = \int_0^{\min(\tau,\tau_{k-1})} \tilde{Q}'_{q,m}(\tau')d\tau' \tag{38}$$

$$\Phi'_{q,k,m}(\tau_k - \tau_{k'}) = \frac{f_{q,k,m}(\tau_k - \tau_{k'-1}) - f_{q,k,m}(\tau_k - \tau_{k'})}{\tau_{k'} - \tau_{k'-1}} \tag{39}$$

where $f_{q,k,m}$ is the accumulated heat extracted by the m-th segment evaluated at time τ_k and $\Phi'_{q,k,m}$ is the reconstructed load history of the m-th segment at time τ_k.

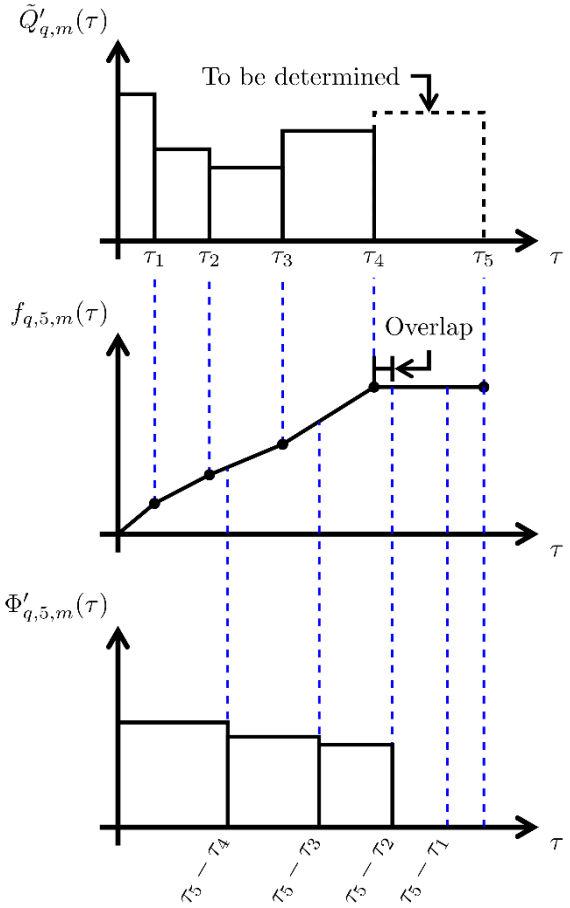

Figure 4. Load history reconstruction

The proposed method limits the use of interpolation by interpolating the accumulated heat extracted instead of the thermal response factors, thereby reducing the number of interpolations by a factor N_q compared to the previous scheme. Linear interpolation is used instead of cubic spline interpolation since the heat extraction rates are stepwise constant and linear interpolation thus conserves thermal energy.

As shown in Figure 4, the proposed load history reconstruction method may cause the reconstructed load to overlap with the heat extraction rate to be determined. At any time τ_k, an overlap exists if there is no previous time $\tau_{k'}$ for which $\tau_{k'} = \tau_k - \tau_{k-1}$. To minimize this overlap, the time-step should be monotonically increasing. Here, two different monotonically

increasing time-stepping schemes are considered. First, the load aggregation cell size of Claesson and Javed (2012) can be used to define time-steps:

$$\tau_k = \sum_{k'=1}^{k} 2^{v-1}\Delta\tau \tag{40}$$

$$v = \text{ceil}\left(k'/n_{steps}\right) \tag{41}$$

where $\Delta\tau$ is the initial time-step and $\text{ceil}(x)$ is the ceiling rounded value of x. The time-step size doubles every n_{steps} time-steps.

Second, a geometrically expanding time-stepping scheme can be used to define time-steps:

$$\tau_k = \sum_{k'=1}^{k} \Delta\tau \cdot r^{(k'-1)} = \Delta\tau \frac{1-r^{k'}}{1-r} \tag{42}$$

where r is a geometric a geometric expansion coefficient that satisfies the relation:

$$\tau_{N_t} = \tau_{max} = \Delta\tau \frac{1-r^{N_t}}{1-r} \tag{43}$$

where $\tau_{max} = t_{max}/t_s$ is the maximum value of the dimensionless time.

The overlap also means that the value of the thermal response factor matrix in Equation (17) may not be known for a given time $\tau_k - \tau_{k-1}$. In the proposed method, linear interpolation is used to evaluate the matrix at these times from the known values. Alternatively, these values could be calculated *a priori* for a given distribution of time-steps (e.g. Equation (40)). However, as will be seen in the results section, the error attributed to linear interpolation in the proposed load history reconstruction method is minimal.

3.3. Multiprocessing

Both the identification of similarities and the evaluation of thermal response factors present independent tasks that can be executed in parallel, making use of multicore processors. In the identification of similarities, the similarities for each of the distance groups are independent from each other and can be identified simultaneously. In the evaluation of segment-to-segment thermal response factors, the values for a given pair of segments at different time-steps can also be evaluated simultaneously. The proposed method for the calculation of g-functions was implemented into Python and multiple processes are used during these two tasks.

4. Results

4.1. Similarities in the evaluation of the finite line source solution

The computational performance and the accuracy of the proposed methodology is tested in the calculation of g-functions of various bore field configurations as shown on Figure 5: (a) rectangular, (b) box-shaped, (c) L-shaped and (d) U-shaped. In all considered cases, the g-functions were calculated for a borehole length $L = 150$ m, a borehole radius $r_b = 0.075$ m ($r_b/L = 0.0005$), a buried depth $D = 4$ m ($D/L = 0.027$) and a uniform spacing $B = 7.5$ m ($B/L = 0.05$). All boreholes are divided into $n_q = 12$ segments. The initial time-step is $\Delta t = 1$ h and the maximum time is 1,000 years. The time-steps are defined by Equation (40) with $n_{steps} = 6$ time-steps, for a total of $N_t = 128$ time-steps. g-Functions were evaluated for all bore field configurations with sizes ranging from 1 × 1 to 12 × 12 using similarities and from 1 × 1 to 8 × 8 without using similarities. For the identification of similarities in the bore fields, an absolute tolerance $\varepsilon_{d,abs} = 0.15$ m and a relative tolerance $\varepsilon_{s,rel} = \varepsilon_{d,rel} = 1 \times 10^{-6}$ were used.

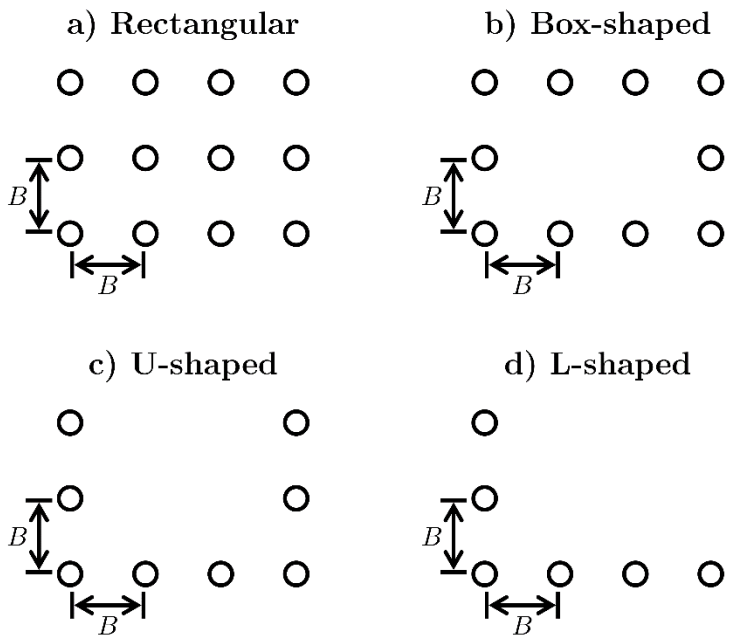

Figure 5. (a) Rectangular, (b) box-shaped, (c) U-shaped and (d) L-shaped fields of 4 × 3 boreholes

The proposed methodology is first validated against the method of Cimmino and Bernier (2014) on Figure 6 for rectangular fields of 3 × 2, 6 × 4 and 10 × 10 boreholes. The maximum observed absolute differences between the results using the proposed methodology and that of Cimmino and Bernier are 0.11 %, 0.38 % and 1.01 % for the 3 × 2, 6 × 4 and 10 × 10 bore fields, respectively. The proposed methodology is also validated against the numerical finite difference model of Eskilson (1987). Figure 7 shows a comparison between the numerically and analytically calculated g-functions of all rectangular fields at a time $\ln(t/t_s) = -1$. The maximum absolute difference is 5.1 % for a rectangular field of 12 × 12 boreholes.

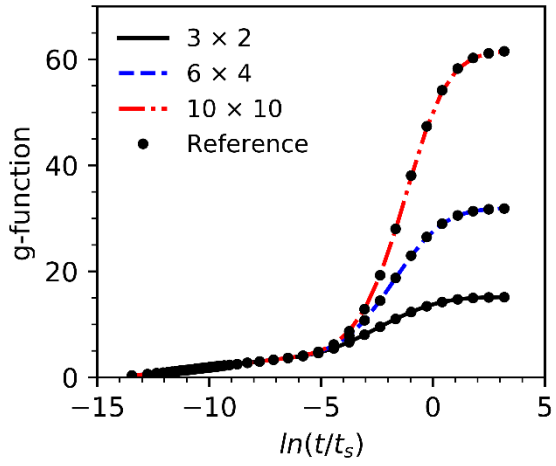

Figure 6. g-Functions of rectangular fields of 3 × 2, 6 × 4 and 10 × 10 boreholes

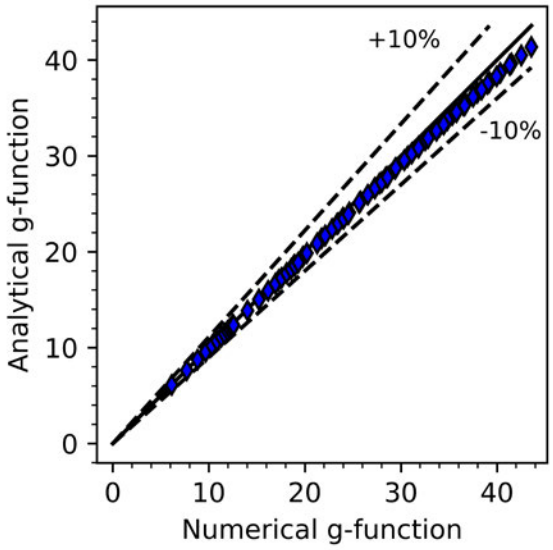

Figure 7. Numerical validation of the g-function values of rectangular fields at ln(t/ts) = -1.0

Figure 8 compares the calculation time with and without the proposed similarity identification method. All calculations were executed on the same computer equipped with a 4.2 GHz quad core (8 threads) processor using only one of the processor cores. As shown on Figure 8a, when not using similarities, the calculation time is proportional to $N_b(N_b + 1)$. The computational advantage of the similarity identification method, defined as the ratio of the

calculation times without and with the proposed similarity identification method, is presented on Figure 8b. For the considered cases, the proposed method provides a reduction of calculation time between a factor 4.7 for a single borehole and a factor 308 for a rectangular field of 8 × 8 boreholes. The computational advantage varies with the bore field configuration. The rectangular configuration offers the greatest reduction since it is the most densely packed and features two planes of symmetry. For instance, the calculation time for a rectangular field of 7 × 7 boreholes is 191 seconds when using the similarity identification method and 12.95 hours without. In this case, the calculation time is then reduced by a factor 244, more than 2 orders of magnitude.

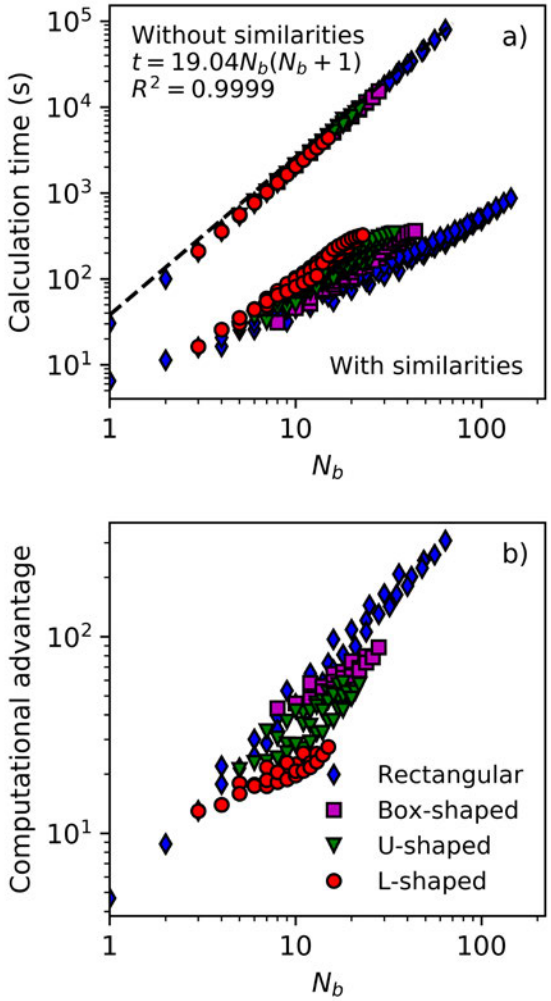

Figure 8. (a) Calculation time and (b) computational advantage of the similarity identification method

4.2. Load history reconstruction

The influence of the time-step on the accuracy of the g-function evaluation is evaluated for a rectangular field of 7 × 7 boreholes ($N_b = 49$). The g-function of this bore field was calculated using the two previously introduced time-stepping schemes with a value of $n_{steps} = 6$ (i.e. $N_t = 128$) for the scheme presented in Equation (40) and with the same values of Δt, t_{max} and N_t for the scheme presented in Equation (42). Both time-stepping grids are refined twice by dividing each of the time-steps into two equal parts to create grids of N_t = 256 and N_t = 512 time-steps for both time-stepping schemes. The time-step independent values of the g-function is obtained by Richardson extrapolation:

$$g_{extrap}(t_k) = g_{512}(t_k) + \frac{g_{512}(t_k) - g_{256}(t_k)}{2^q - 1} \tag{44}$$

$$q = \ln\left(\frac{g_{128}(t_k) - g_{256}(t_k)}{g_{256}(t_k) - g_{512}(t_k)}\right) / \ln(2) \tag{45}$$

where g_{extrap} is the Richardson extrapolated value of the g-function, g_{N_t} is the g-function evaluated with N_t time-steps and q is the observed order of accuracy.

The differences between the g-functions and the extrapolated values are presented on Figure 9a. The maximum difference appears near $\ln(t/t_s) = -1$ for all considered time-stepping grids. The maximum differences with N_t = 128, 256 and 512 are 0.20 %, 0.13 % and 0.098 % using the time-stepping scheme of Equation (40) and 0.16 %, 0.095 % and 0.067 % using the time-stepping scheme of Equation (42). To further analyse the influence of the time-steps on the

accuracy of the g-function, the g-function was calculated without the temporal superposition of loads. At any time t_k, the g-function is evaluated as if that time was the first time-step and heat extraction rates at all segments were constant from time $t = 0$ to time t_k. The differences with the extrapolated g-function are shown on Figure 9b. The maximum difference is 2.7 % at $\ln(t/t_s) = -1.5$.

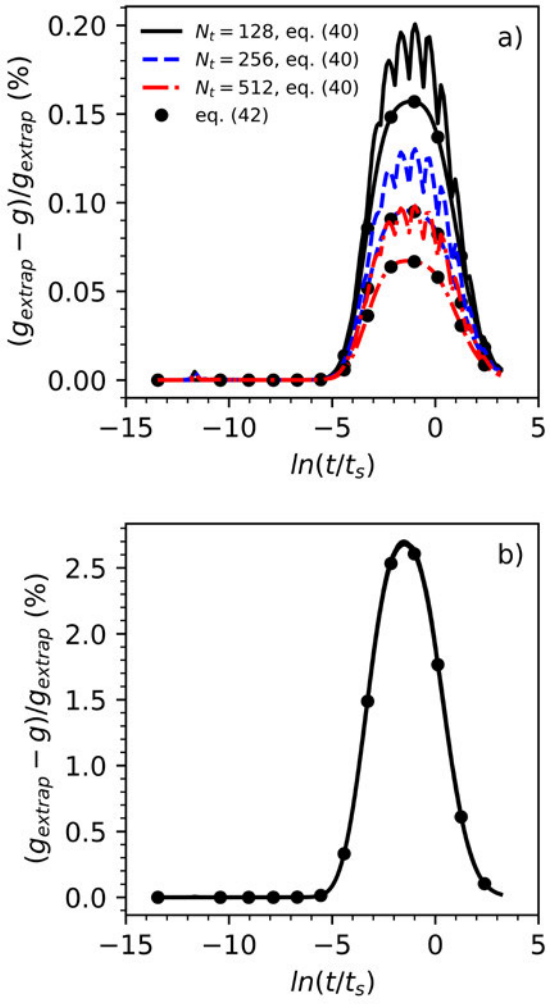

Figure 9. Relative differences with the time-step independent g-function (a) with and (b) without temporal superposition

4.3. Multiprocessing

Table 1 compares the calculation time for rectangular fields of 5 × 5, 7 × 7 and 10 × 10 boreholes using 1, 2 and 4 parallel processes for the identification of similarities and the evaluation of the segment-to-segment response factors. It is shown that the calculation time decreases by a factor 2.4, 1.9 and 1.5 when using 4 processes for the fields of 5 × 5, 7 × 7 and 10 × 10 boreholes, respectively. The decrease in calculation time decreases as the number of boreholes increases since not all tasks involved in the calculation of the g-function benefit from the multiple processor cores. The load history reconstruction method (Equation (39)), the temporal superposition (Equation (37)) and the solution of the system of equations (Equation (20)) are all done using only one process. Figure 10 shows the ratio between the calculation times using 1 and 4 processes for all considered bore fields. It is shown that the ratio of calculation time varies between 1.3 and 3.1.

Table 1. Calculation times using multiple processes (in seconds)

	1 process	2 processes	4 processes
5 × 5 ($N_b = 25$)	87.2	54.7	36.9
7 × 7 ($N_b = 49$)	189.4	128.9	98.2
10 × 10 ($N_b = 100$)	493.9	389.9	333.5

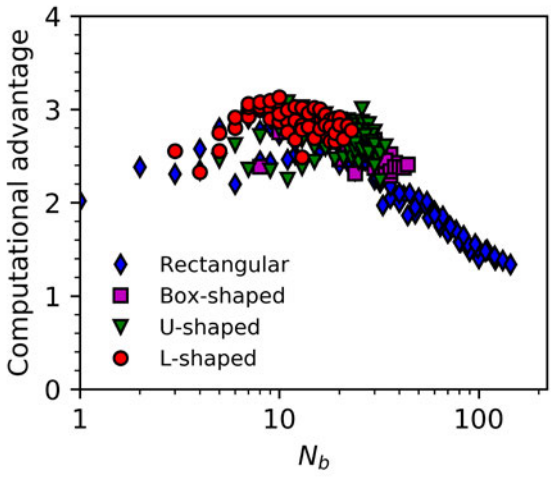

Figure 10. Computational advantage of using multiple processes

4.4. Irregular bore field configurations

The proposed methodology is tested in the evaluation of the g-functions of irregular bore field configurations with large amounts of boreholes. g-Functions are evaluated for fields of N_b = 8, 16, 32, 64, 128, 256 and 512 boreholes. Boreholes are randomly positioned in a W by W square domain with $W = \bar{B}\left(\sqrt{N_b} - 1\right)$, where $\bar{B}$ = 7.5 m is the target mean adjacent distance between boreholes. The boreholes are positioned so that the minimum distance between two boreholes is greater than 3 m. The g-functions are evaluated with Δt = 1 h, t_{max} = 2000 years, N_t = 25 and α_s = 10^{-6} m^2/s using the time-stepping scheme of Equation (42). The g-function curves and the calculation time for all bore fields are shown on Figures 11a and 11b. The borehole positions in the field of N_b = 512 boreholes are shown on Figure 11c. It is shown that the g-function of the field of N_b = 512 boreholes is calculated in 27 minutes. Extrapolating from the results presented on Figure 8 without the use of similarities to evaluate segment-to-segment thermal response factors, the calculation time for the evaluation of the g-function of the same bore field would be of the order of 10 days.

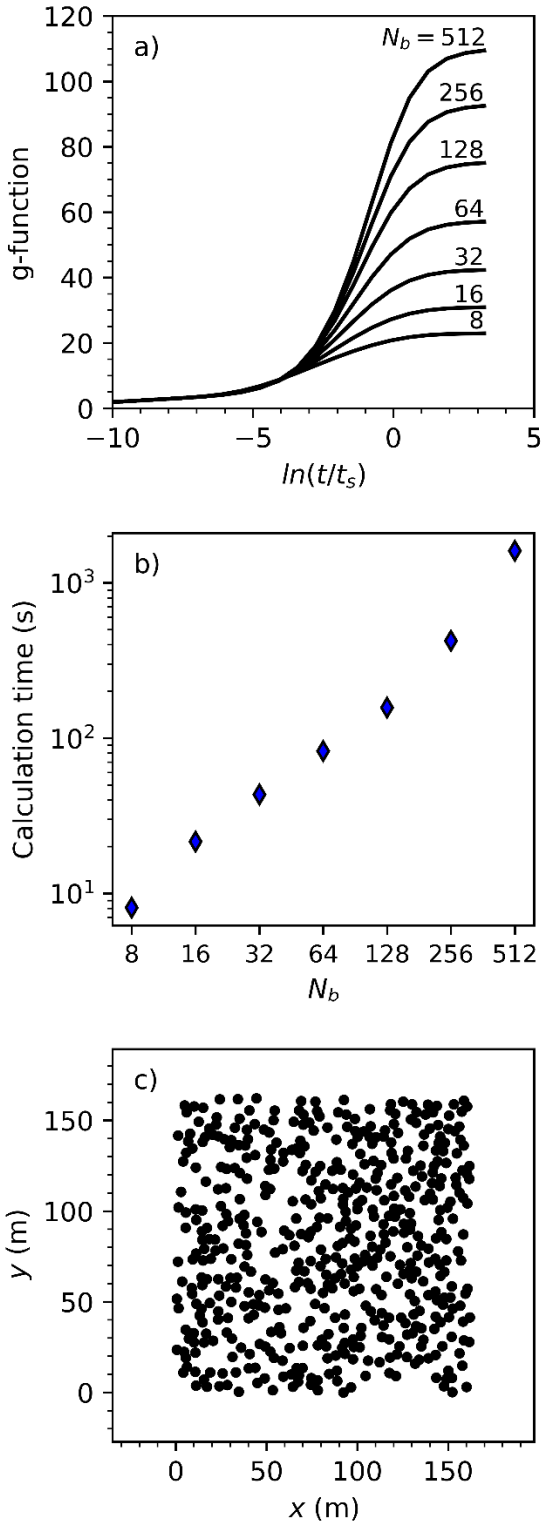

Figure 11. (a) g-Functions and (b) calculation times of randomly positioned bore fields, (c) field of N_b = 512 boreholes

5. Conclusion

The g-function of a given geothermal bore field is obtained by the temporal and spatial superposition of the finite line source solution. To ensure a uniform borehole wall temperature along the borehole lengths, equal for all boreholes, it is necessary to divide each borehole into a number of finite line source segments. The finite line source solution must be evaluated for all pairs of line source segments in the bore field. The number of required evaluations of the finite line source solution increases with the square of the number of boreholes. This process becomes rapidly time consuming and the g-functions can take several hours to calculate.

Numerical methods for the efficient calculation of g-functions were presented. Similarities in the evaluation of the finite line source solution are identified to reduce the number of evaluations of the finite line source solution. Similar pairs of finite line source segments yield the same value of the finite line source solution. Using the presented load history reconstruction method, it is possible to evaluate the g-function using a variable time-step without the need to evaluate the finite line source solution at intermediate values of time. The proposed similarity identification method permits the use of multiple processes.

g-Functions were evaluated for rectangular, box-shaped, U-shaped and L-shaped bore fields of size ranging from 1×1 to 12×12. For these considered cases, the similarity identification method reduced the required calculation time by a factor of 4.7 to 308, with larger bore fields having a larger reduction in calculation time. Using 4 processes, the calculation time is further reduced by a factor of 1.3 to 3.1. For instance, the g-function of a rectangular 7×7 bore field is evaluated in 12.95 hours without any of the proposed methods and in 98.2 seconds using the proposed methods and 4 processes. The proposed numerical methods also make possible the evaluation of g-functions for large bore fields in irregular configurations. The

g-function of a field of 512 randomly positioned boreholes was evaluated in 27 minutes. The proposed numerical methods provide a viable alternative to pre-calculated g-functions and allow for the fast calculation of g-functions for custom bore fields prior to simulation.

The application of the presented numerical methods is not limited to the evaluation of g-functions using the finite line solution. The similarity identification method can be applied to any problem that requires the evaluation of the thermal response factor matrix. For instance, this matrix is needed in network-based simulation methods for geothermal systems to evaluate the temperature response of individual boreholes (Lazzarotto 2014; Lamarche 2017a; Cimmino 2017). The similarity identification can also be applied to other analytical solutions, such as the moving finite line source solution (Molina-Giraldo et al. 2011) and the piecewise-linear finite line source solution (Lamarche 2017b), provided suitable conditions are imposed in the identification of similarities.

Acknowledgements

The author received a start-up subsidy from the *Fonds de recherche du Québec – Nature et Technologie* (FRQNT).

References

Abdelaziz, S. L., T. Y. Ozudogru, C. G. Olgun, and J. R. Martin. 2014. "Multilayer Finite Line Source Model for Vertical Heat Exchangers." *Geothermics* 51 (July): 406–416. doi:10.1016/j.geothermics.2014.03.004.

Bernier, M., P. Pinel, R. Labib, and R. Paillot. 2004. "A Multiple Load Aggregation Algorithm for Annual Hourly Simulations of GCHP Systems." *HVAC&R Research* 10 (4): 471–487. doi:10.1080/10789669.2004.10391115.

Cimmino, M. 2017. "A Finite Line Source Simulation Model for Geothermal Systems with Series- and Parallel-Connected Boreholes and Independent Fluid Loops." *Journal of*

Building Performance Simulation, October, 1–19. doi:10.1080/19401493.2017.1381993.

Cimmino, M. 2015. "The Effects of Borehole Thermal Resistances and Fluid Flow Rate on the G-Functions of Geothermal Bore Fields." *International Journal of Heat and Mass Transfer* 91: 1119–1127. doi:10.1016/j.ijheatmasstransfer.2015.08.041.

Cimmino, M., and M. Bernier. 2013. "Preprocessor for the Generation of G-Functions Used in the Simulation of Geothermal Systems." In *Proceedings of BS2013: 13th Conference of International Building Performance Simulation Association*, 2675–2682. Chambery: IBPSA.

Cimmino, M., and M. Bernier. 2014. "A Semi-Analytical Method to Generate G-Functions for Geothermal Bore Fields." *International Journal of Heat and Mass Transfer* 70 (c): 641–650. doi:10.1016/j.ijheatmasstransfer.2013.11.037.

Cimmino, M., M. Bernier, and F. Adams. 2013. "A Contribution towards the Determination of G-Functions Using the Finite Line Source." *Applied Thermal Engineering* 51 (1–2): 401–412. doi:10.1016/j.applthermaleng.2012.07.044.

Claesson, J., and S. Javed. 2011. "An Analytical Method to Calculate Borehole Fluid Temperatures for Time-Scales from Minutes to Decades." *ASHRAE Transactions* 117 (2): 279–288.

Claesson, J., and S. Javed. 2012. "A Load-Aggregation Method to Calculate Extraction Temperatures of Borehole Heat Exchangers." *ASHRAE Transactions* 118 (1): 530–539.

Cui, P., H. Yang, and Z. Fang. 2006. "Heat Transfer Analysis of Ground Heat Exchangers with Inclined Boreholes." *Applied Thermal Engineering* 26 (11–12): 1169–1175. doi:10.1016/j.applthermaleng.2005.10.034.

Eskilson, P. 1987. "Thermal Analysis of Heat Extraction Boreholes." University of Lund.

Fisher, D., S. Rees, S. K. Padhmanabhan, and A. Murugappan. 2006. "Implementation and Validation of Ground-Source Heat Pump System Models in an Integrated Building and System Simulation Environment." *HVAC&R Research* 12 (S1): 693–710. doi:10.1080/10789669.2006.10391201.

Fossa, M. 2011. "The Temperature Penalty Approach to the Design of Borehole Heat

Exchangers for Heat Pump Applications." *Energy and Buildings* 43 (6): 1473–1479. doi:10.1016/j.enbuild.2011.02.020.

Hellström, G., and B. Sanner. 1994. "Software for Dimensioning of Deep Boreholes for Heat Extraction." In *Proceedings of Calorstock*, 94:195–202. Espoo-Helsinki, Finland.

Hu, J. 2017. "An Improved Analytical Model for Vertical Borehole Ground Heat Exchanger with Multiple-Layer Substrates and Groundwater Flow." *Applied Energy* 202 (September): 537–549. doi:10.1016/j.apenergy.2017.05.152.

Lamarche, L. 2011. "Analytical G-Function for Inclined Boreholes in Ground-Source Heat Pump Systems." *Geothermics* 40 (4): 241–249. doi:10.1016/j.geothermics.2011.07.006.

Lamarche, L. 2017a. "Mixed Arrangement of Multiple Input-Output Borehole Systems." *Applied Thermal Engineering*. doi:10.1016/j.applthermaleng.2017.06.060.

Lamarche, L. 2017b. "G-Function Generation Using a Piecewise-Linear Profile Applied to Ground Heat Exchangers." *International Journal of Heat and Mass Transfer* 115 (December): 354–360. doi:10.1016/j.ijheatmasstransfer.2017.08.051.

Lamarche, L, and B Beauchamp. 2007. "A New Contribution to the Finite Line-Source Model for Geothermal Boreholes." *Energy and Buildings* 39 (2): 188–198. doi:10.1016/j.enbuild.2006.06.003.

Lazzarotto, A. 2014. "A Network-Based Methodology for the Simulation of Borehole Heat Storage Systems." *Renewable Energy* 62: 265–275. doi:10.1016/j.renene.2013.07.020.

Lazzarotto, A. 2016. "A Methodology for the Calculation of Response Functions for Geothermal Fields with Arbitrarily Oriented Boreholes – Part 1." *Renewable Energy* 86: 1380–1393. doi:10.1016/j.renene.2015.09.056.

Lazzarotto, A., and F. Björk. 2016. "A Methodology for the Calculation of Response Functions for Geothermal Fields with Arbitrarily Oriented Boreholes – Part 2." *Renewable Energy* 86: 1353–1361. doi:10.1016/j.renene.2015.09.057.

Li, M., and A. C. K. Lai. 2012. "Heat-Source Solutions to Heat Conduction in Anisotropic Media with Application to Pile and Borehole Ground Heat Exchangers." *Applied Energy* 96 (August): 451–458. doi:10.1016/j.apenergy.2012.02.084.

Liu, X. 2005. “Development and Experimental Validation of Simulation of Hydronic Snow Melting Systems for Bridges.” Oklahoma State University.

Liu, X., and G. Hellström. 1999. “Enhancements of an Integrated Simulation Tool for Ground-Source Heat Pump System Design and Energy Analysis.” In *Proc. 10th International Conference on Thermal Energy Storage*. Galloway (NJ), USA.

Malayappan, V., and J. D. Spitler. 2013. “Limitations of Using Uniform Heat Flux Assumptions in Sizing Vertical Borehole Heat Exchanger Fields.” In *Proceedings of Clima 2013*, 16–19. Prague, Czech Republic.

Marcotte, D., and P. Pasquier. 2009. “The Effect of Borehole Inclination on Fluid and Ground Temperature for GLHE Systems.” *Geothermics* 38 (4): 392–398. doi:10.1016/j.geothermics.2009.06.001.

Marcotte, D., and P. Pasquier. 2014. “Unit-Response Function for Ground Heat Exchanger with Parallel, Series or Mixed Borehole Arrangement.” *Renewable Energy* 68: 14–24. doi:10.1016/j.renene.2014.01.023.

Molina-Giraldo, N., P. Blum, K. Zhu, P. Bayer, and Z. Fang. 2011. “A Moving Finite Line Source Model to Simulate Borehole Heat Exchangers with Groundwater Advection.” *International Journal of Thermal Sciences* 50 (12): 2506–2513. doi:10.1016/j.ijthermalsci.2011.06.012.

Spitler, J. D. 2000. “A Design Tool for Commercial Building Ground Loop Heat Exchangers.” In *Proceedings of the Fourth International Heat Pumps in Cold Climates Conference*. Aylmer (QC), Canada.

Zeng, H. Y., N. R. Diao, and Z. H. Fang. 2002. “A Finite Line-Source Model for Boreholes in Geothermal Heat Exchangers.” *Heat Transfer - Asian Research* 31 (7): 558–567. doi:10.1002/htj.10057.

Appendix A. Algorithm 1: Identification of distance groups

This algorithm creates groups of pairs of borehole segments. All pairs in a distance group share the same separation distance within the prescribed tolerance.

Input: $(x_{q,m}, y_{q,m})$: the coordinates of the borehole segments

$r_{q,m}$: the radius of the borehole segments

N_q: the number of borehole segments

$\varepsilon_{d,rel}$: the relative tolerance on the distances when equal to the radius

$\varepsilon_{d,abs}$: the absolute tolerance on the distances

Output: N_d: the number of distance groups

$d^{(w)}$: the distance associated with each distance group w

$n_d^{(w)}$: the number of segment pairs in each distance group w

$P_d^{(w,p)}$: the segment indices of each pair p in each distance group w

Initialize: $N_d \leftarrow 1$, $d^{(1)} \leftarrow r_{q,1}$, $n_d^{(1)} \leftarrow 0$

Cycle through all segment pairs (m, n)

for $m = 1, \dots, N_q$:

for $n = m, \dots, N_q$:

Calculate the distance between segments m *and* n

$d' = \sqrt{(x_{q,m} - x_{q,n})^2 + (y_{q,m} - y_{q,n})^2}$; $\Delta d = \varepsilon_{d,abs}$

if $d' < r_{q,m}$ **then**:

$d' = r_{q,m}$; $\Delta d = \varepsilon_{d,rel} r_{q,m}$

Find or create a new distance group for segment pair (m, n)

for $w = 1, \dots, N_d$:

if $|d' - d^{(w)}| < \Delta d$ **then**:

Add segment pair (m, n) *to distance group* k

$n_d^{(w)} \leftarrow n_d^{(w)} + 1$; $P_d^{\left(w,n_d^{(w)}\right)} \leftarrow (m,n)$

break for loop

else if $k = N_d$ **then**:

Create new distance group for segment pair (m,n)

$N_d \leftarrow N_d + 1$; $d^{(N_d)} \leftarrow d'$; $n_d^{(N_d)} \leftarrow 1$; $P_d^{(N_d,1)} \leftarrow (m,n)$

Return

Appendix B. Algorithm 2: Identification of similarity groups

This algorithm separates each of the identified distance groups into similarity groups. All pairs in a similarity group share the same segment-to-segment thermal response factor. The algorithm is described for the identification of similarities of the real segment-to-segment thermal response factors. The identification of similarities for the image segment-to-segment thermal response factors follows the same process, but the borehole segment pairs need to be tested for condition (I2) rather than condition (R2).

Input: $L_{q,m}$: the length of each borehole segment m

$D_{q,m}$: the buried depth of each borehole segment m

N_d: the number of distance groups

$d^{(w)}$: the distance associated with each distance group w

$n_d^{(w)}$: the number of segment pairs in each distance group w

$P_d^{(w,p)}$: the segment indices in each pair p of each distance group w

$\varepsilon_{s,rel}$: the relative tolerance

Output: $N_{s,real}^{(w)}$: the number of similarity groups in each distance group w

$n_{s,real}^{(w,s)}$: the number of segment pairs in each similarity group s of each distance group w

$P_{s,real}^{(w,s,p)}$: the segment indices in each pair p of each similarity group s of each distance group w

$\left(L_{s,real,1}^{(w,s)}, L_{s,real,2}^{(w,s)}\right)$: the length of the borehole segments in each similarity group s of each distance group w

$\left(D_{s,real,1}^{(w,s)}, D_{s,real,2}^{(w,s)}\right)$: the buried depth of the borehole segments in each similarity group s of each distance group w

Identify similarity groups within each distance group

for $w = 1, \dots, N_d$:

Initialize the first similarity group in distance group k to the first segment pair

$(m, n) = P_d^{(w,1)}$

$N_{s,real}^{(w)} \leftarrow 1$; $n_{s,real}^{(w,1)} \leftarrow 1$; $P_{s,real}^{(w,1,1)} \leftarrow P_d^{(w,1)}$; $\left(L_{s,real,1}^{(w,1)}, L_{s,real,2}^{(w,1)}\right) \leftarrow \left(L_{q,m}, L_{q,n}\right)$;

$\left(D_{s,real,1}^{(w,1)}, D_{s,real,2}^{(w,1)}\right) \leftarrow \left(D_{q,m}, D_{q,n}\right)$

For each pair (m, n) in distance group k, find or create a new similarity group

for $p = 2, \dots, n_d^{(w)}$:

$(m, n) = P_d^{(w,p)}$

for $s = 1, \dots, N_{s,real}^{(w)}$:

if $\left|L_{s,real,1}^{(w,s)} - L_{q,m}\right| < \varepsilon_{s,rel} L_{s,real,1}^{(w,s)}$ **and** $\left|L_{s,real,2}^{(w,s)} - L_{q,n}\right| < \varepsilon_{s,rel} L_{s,real,2}^{(w,s)}$ **and** $\left|\left(D_{s,real,1}^{(w,s)} - D_{s,real,2}^{(w,s)}\right) - \left(D_{q,m} - D_{q,n}\right)\right| < \varepsilon_{s,rel}\left|D_{s,real,1}^{(w,s)} - D_{s,real,2}^{(w,s)}\right|$ **then**:

Add pair (m, n) to similarity group s of distance group w

$n_{s,real}^{(w,s)} \leftarrow n_{s,real}^{(w,s)} + 1$; $P_{s,real}^{(w,s,n_{s,real}^{(w,s)})} \leftarrow (m,n)$

break for loop

else if $\left|L_{s,real,1}^{(w,s)} - L_{q,n}\right| < \varepsilon_{s,rel} L_{s,real,1}^{(w,s)}$ **and** $\left|L_{s,real,2}^{(w,s)} - L_{q,m}\right| < \varepsilon_{s,rel} L_{s,real,2}^{(w,s)}$ **and** $\left|\left(D_{s,real,1}^{(w,s)} - D_{s,real,2}^{(w,s)}\right) - \left(D_{q,n} - D_{q,m}\right)\right| < \varepsilon_{s,rel}\left|D_{s,real,1}^{(w,s)} - D_{s,real,2}^{(w,s)}\right|$ **then**:

Add pair (n,m) *to similarity group* s *of distance group* w

$n_{s,real}^{(w,s)} \leftarrow n_{s,real}^{(w,s)} + 1$; $P_{s,real}^{(w,s,n_{s,real}^{(w,s)})} \leftarrow (n,m)$

break for loop

else if $s = N_{s,real}^{(w)}$ **then**:

Create new similarity group for segment pair (m,n)

$N_{s,real}^{(w)} \leftarrow N_{s,real}^{(w)} + 1$; $n_{s,real}^{\left(w,N_{s,real}^{(w)}\right)} \leftarrow 1$; $P_{s,real}^{\left(w,N_{s,real}^{(w)},1\right)} \leftarrow (m,n)$;

$\left(L_{s,real,1}^{\left(w,N_{s,real}^{(w)}\right)}, L_{s,real,2}^{\left(w,N_{s,real}^{(w)}\right)}\right) \leftarrow \left(L_{q,m}, L_{q,n}\right)$; $\left(D_{s,real,1}^{\left(w,N_{s,real}^{(w)}\right)}, D_{s,real,2}^{\left(w,N_{s,real}^{(w)}\right)}\right) \leftarrow \left(D_{q,m}, D_{q,n}\right)$

Return

Appendix C. Algorithm 3: Evaluation of segment-to-segment thermal response factors

This algorithm evaluates the segment-to-segment thermal response factors for each similarity group and assigns the values to all borehole segment pairs within the similarity group.

Input: N_t: the number of time-steps

t_k: the time value of each time-step k

N_d: the number of distance groups

$N_{s,real}^{(w)}$: the number of similarity groups in each distance group w

$n_{s,real}^{(w,s)}$: the number of segment pairs in each similarity group s of each distance group w

$P_{s,real}^{(w,s,p)}$: the segment indices in each pair p of each similarity group s of each distance group w

$d^{(w)}$: the distance associated with each distance group w

$\left(L_{s,real,1}^{(w,s)}, L_{s,real,2}^{(w,s)}\right)$: the length of the borehole segments in each similarity group s of each distance group w

$\left(D_{s,real,1}^{(w,s)}, D_{s,real,2}^{(w,s)}\right)$: the buried depth of the borehole segments in each similarity group s of each distance group w

Output: $h_{q,m,n}^{real}(t_k)$: the value of the segment-to-segment thermal response factor for all pairs (m, n) at all times t_k

Cycle through all symmetry groups

for $w = 1, \dots, N_d$:

for $s = 1, \dots, N_{s,real}^{(w)}$:

Calculate the segment-to-segment response factor for the first pair in similarity group s of distance group w

$(m, n) = P_{s,real}^{(w,s,1)}$; $\left(L_{q,m}, L_{q,n}\right) = \left(L_{s,real,1}^{(w,s)}, L_{s,real,2}^{(w,s)}\right)$; $\left(D_{q,m}, D_{q,n}\right) = \left(D_{s,real,1}^{(w,s)}, D_{s,real,2}^{(w,s)}\right)$

for $k = 1, \dots, N_t$:

evaluate $h_{q,m,n}^{real}(t_k)$ from Equation (3)

$h_{q,n,m}^{real}(t_k) = \frac{L_{q,m}}{L_{q,n}} h_{q,m,n}^{real}(t_k)$

Apply the values to all other pairs in similarity group s of distance group w

for $p = 2, \ldots., n_{s,real}^{(w,s)}$:

$$(m', n') = P_{s,real}^{(w,s,p)}; h_{q,m',n'}^{real}(t_k) = h_{q,m,n}^{real}(t_k); h_{q,n',m'}^{real}(t_k) = h_{q,n,m}^{real}(t_k)$$

Return